Dependence of the optical activity of nano-sculptured copper thin films on the structural parameters and the dispersion of the dielectric function

F. Babaei[1], H. Savaloni[2,*]

[1]*Department of Physics, University of Qom, Qom, Iran.*
[2]*Department of Physics, University of Tehran, North-Kargar Street, Tehran, Iran.*

Abstract

Influence of the structural parameters (namely, angle of rise, half structural period, volume fraction of metal inclusion, columns shape factor, thickness) and the dielectric dispersion function on the optical activity of axially excited chiral nano-sculptured copper thin films are investigated for both s and p linearly polarized lights, using Bruggeman homogenization formalism in conjunction with the experimentally available relative dielectric constants for the bulk copper. It is observed that for both s and p polarizations the maximum of optical activity shifts towards longer wavelengths with increasing the half structural period, volume fraction of metal inclusion and the film thickness, while it shifts towards shorter wavelengths with increasing the transverse aspect ratio of the columns. The circular Bragg phenomenon is clearly observed when the angle of rise increased from 20° to 45°. Comparison of spectral results shows that the dispersion of the dielectric function has a considerable effect on the results.

1. Introduction

Chiral sculptured thin films (CSTFs) are three dimensional structures that may be produced by using glancing angle deposition technique (GLAD) combined with the rotation of substrate about its normal to surface axis [1]. The intriguing feature in CSTFs is due to appearance of circular Bragg phenomenon in these structures [2]. By utilizing the circular Bragg phenomenon, chiral STFs as circular polarization filters have been theoretically examined and then experimentally realized [2,3]. A handedness–selective light inverter, which comprises a chiral STF and a CTF functioning as a half wave-plate, was also designed and then fabricated and tested [4,5]. By introducing either a layer defect or a twist defect in the middle of a chiral STF, narrowband spectral–hole filters have been designed and implemented [6-8].
In early 1996 the optical activity of these films (the rotation of the linear polarized light in the plane of polarization of light) similar to cholestric liquid crystals and other chiral structures was observed [9]. When a linearly polarized light is incident on a CSTF structure, the transmitted light experiences a rotation in the polarization plane. This optical rotation is a function of wavelength of light in vacuum, which is called optical activity. Optical activity spectra are usually used for materials spectroscopy analysis [10].

*Corresponding author: Hadi Savaloni;
 E-mail: savaloni@khayam.ut.ac.ir
 Tel: (+90) 21 88635776
 Fax: (+90) 21 88004781

The occurrence of circular Bragg phenomenon can be deduced from circular reflectance and transmission. However, other characteristics such as optical activity can also be used for this reason [10]. In our earlier works the occurrence of circular Bragg phenomenon in circular reflectance and transmission spectra are reported [11,12]. In this work our aim is to calculate the optical activity of chiral sculptured copper thin films, using the Bruggman homogenization formalism [13,14] and eigen- value method [11,12,15] and investigate its dependence on different structural parameters and dispersion of the dielectric function.

2. Theory

Assume that the $(0 \le z \le d)$ space is occupied by a metallic chiral STF with a permittivity dyadic of (Fig. 1) [11]:

$$\underline{\underline{\varepsilon}}(\underline{r}) = \varepsilon_0 \underline{\underline{S}}_z(z) \cdot \underline{\underline{S}}_y(\chi) \cdot \left[\varepsilon_a \underline{u}_z \underline{u}_z + \varepsilon_b \underline{u}_x \underline{u}_x + \varepsilon_c \underline{u}_y \underline{u}_y\right] \cdot \underline{\underline{S}}_y^{-1}(\chi) \cdot \underline{\underline{S}}_z^{-1}(z), \tag{1}$$

vectors are underlined, dyadics are double underlined, χ is the angle of rise. The relative permittivity scalars $\varepsilon_a, \varepsilon_b, \varepsilon_c$ are implicit functions of frequency. $\underline{u}_x, \underline{u}_y$ and $\underline{u}_z$ are unit vectors in the Cartesian coordinate system. The tilt dyadic [11]:

$$\underline{\underline{S}}(\chi) = \underline{u}_x \underline{u}_y + \left(\underline{u}_x \underline{u}_x + \underline{u}_z \underline{u}_z\right) \cos \chi + \left(\underline{u}_z \underline{u}_x + \underline{u}_x \underline{u}_z\right) \sin \chi, \tag{2}$$
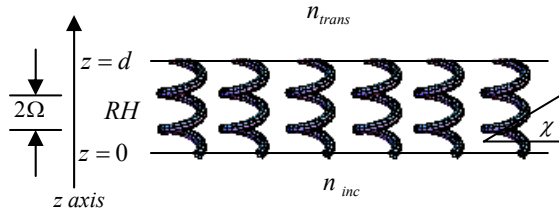
Fig. 1. Schematic of the structural period 2Ω and the angle of rise χ for a right-handed (RH) CSTF.

with $\chi \in (0^{\circ}, 90^{\circ})$ and the rotation dyadic [12]:

$$\underline{\underline{S}}_z(z) = \underline{u}_z\underline{u}_z + (\underline{u}_x\underline{u}_x + \underline{u}_y\underline{u}_y)\cos pz + h(\underline{u}_y\underline{u}_x - \underline{u}_x\underline{u}_y)\sin pz, \tag{3}$$

where $p = \frac{\pi}{\Omega}$, and 2Ω is the structural period. The integers $h = 1$ and $h = -1$ are for the structurally right- and left-handed chiral sculptured thin film, respectively.
Our aim is to obtain the response of electromagnetic plane waves of frequency ω normally fallen on a metallic chiral sculptured thin film slab and the slab is axially being excited. Let the source being positioned at $z = -\infty$. In general form, this plane wave is elliptically polarized. The electric field phasors in vacuous half spaces $Z \le 0$ and $Z \ge d$ are [11,12]:

$$\underline{E}(z) = (a_L\underline{u}_+ + a_R\underline{u}_-)e^{ik_0z} + (a_L\underline{u}_- + r_R\underline{u}_+)e^{-ik_0z},$$
$$Z \le 0 \tag{4}$$

$$\underline{E}(z) = (t_L\underline{u}_+ + t_R\underline{u}_-)e^{ik_0(z-d)}, \qquad Z \ge d. \tag{5}$$

In Eqs. (4) and (5), $\underline{u}_{\pm} = (\underline{u}_x \pm \underline{u}_y)/\sqrt{2}$ are the complex unit vectors and a_L and a_R are the known amplitudes of the left and right-circularly polarized components of the incident plane wave; (r_L and r_R) and (t_L and t_R) are the unknown amplitudes of the reflected and transmitted plane wave (left-circularly polarized (LCP) and (right-circularly polarized (RCP)) components, respectively. The magnetic field phasors in these regions are obtained from:

$$\underline{H}(z) = (i\omega\mu_0)^{-1}\underline{\nabla} \times \underline{E}(z). \tag{6}$$

The phasors of the excited electric and magnetic fields inside the chiral sculptured thin film slab are combined of four axially excited modes in an unbounded chiral sculptured thin film [11]. Therefore, $0 \le z \le d$:

$$\underline{E}(z) = \sum_{n=1}^{4} a_n e^{ig_n z}\{\underline{u}_x [e_{n1}\cos pz - e_{n2}\sin pz]$$
$$+ \underline{u}_y [e_{n1}\sin pz + e_{n2}\cos pz]$$
$$+ \underline{u}_z e_{n3}\}, \qquad 0 \le z \le d \tag{7}$$

$$\underline{H}(z) = \sum_{n=1}^{4} a_n e^{ig_n z}\{\underline{u}_x [h_{n1}\cos pz - h_{n2}\sin pz]$$
$$+ \underline{u}_y [h_{n1}\sin pz + h_{n2}\cos pz]$$
$$+ \underline{u}_z e_{n3}\}, \qquad 0 \le z \le d. \tag{8}$$

In this stage the $a_n, 1 \le n \le 4$ coefficients are unknown and the Cartesian components of the field are given in Eqs. (7) and (8):

$$\left.\begin{array}{r}
e_{n1} = \omega\mu_0\left[g_n^2 - k_0^2\varepsilon_c + p^2\right] \\
e_{n2} = 2ih\omega\mu_0 pg_n \\
e_{n3} = e_{n1}\dfrac{\varepsilon_a - \varepsilon_b}{\varepsilon_a\varepsilon_b}\tilde{\varepsilon}_d\cos\chi\sin\chi \\
h_{n1} = -ihp\left[g_n^2 + k_0^2\varepsilon_c - p^2\right] \\
h_{n2} = g_n\left[g_n^2 + k_0^2\varepsilon_c - p^2\right]
\end{array}\right\}, \tag{9}$$

and the four modal wavelengths are given by:

$$g_1 = -g_3 = 2^{-\frac{1}{2}}\Big\{k_0^2(\varepsilon_c + \tilde{\varepsilon}_d) + 2p^2$$
$$+ k_0[k_0(\varepsilon_c - \tilde{\varepsilon}_d)^2$$
$$+ 8p^2(\varepsilon_c + \tilde{\varepsilon}_d)]^{\frac{1}{2}}\Big\}^{\frac{1}{2}}, \tag{10}$$

$$g_2 = -g_4 = 2^{-\frac{1}{2}}\Big\{k_0^2(\varepsilon_c + \tilde{\varepsilon}_d) + 2p^2$$
$$- k_0[k_0(\varepsilon_c - \tilde{\varepsilon}_d)^2$$
$$+ 8p^2(\varepsilon_c + \tilde{\varepsilon}_d)]^{\frac{1}{2}}\Big\}^{\frac{1}{2}}, \tag{11}$$

$$\tilde{\varepsilon}_d = \frac{\varepsilon_a\varepsilon_b}{\varepsilon_a\cos^2\chi + \varepsilon_b\sin^2\chi}. \tag{12}$$

Here, the possibility of excitation of axially propagating Voigt waves is excluded [11]. Two of these four modal waves propagate in the +z direction and the other two propagate in the -z direction. In order to make decision on the propagation direction of these modal waves, their imaginary part should be examined. The $Im[g_1]$ is always positive, but $Im[g_2]$ in some regions of half structural period becomes negative. In this case, g_2 should be substituted by g_4 [11,12].
In order to determine the values of reflection and transmission a boundary condition should be imposed. The boundary value problem can be applied by considering the continuity of the tangential components of the electrical and magnetic fields' phasors at $z = 0$ and $z = L$. By solving Eq. (13) in matrix form the unknown values for (r_L and r_R) and (t_L and t_R) can be

40

obtained as functions of known values of a_L and a_R [11].

$$\left[\underline{f}(d)\right] = \left[\underline{\underline{B}}(d)\right]\left[\underline{\underline{T}}\right]\left[\underline{\underline{C}}(d)\right]\left[\underline{\underline{T}}\right]^1\left[\underline{f}(0)\right], \tag{13}$$

$$\left[\underline{f}(0)\right] = \frac{1}{\sqrt{2}}\begin{bmatrix} (r_L + r_R) + (a_L + a_R) \\ i[-(r_L - r_R) + (a_L - a_R)] \\ -\frac{i}{\eta_0}[(r_L - r_R) + (a_L - a_R)] \\ -\frac{1}{\eta_0}[(r_L + r_R) - (a_L + a_R)] \end{bmatrix}, \tag{14}$$

$$\left[\underline{f}(L)\right] = \frac{1}{\sqrt{2}}\begin{bmatrix} (t_L + t_R) \\ i(t_L - t_R) \\ -\frac{i}{\eta_0}(t_L + t_R) \\ \frac{1}{\eta_0}(t_L + t_R) \end{bmatrix}, \tag{15}$$

$$\left[\underline{\underline{B}}(L)\right]$$
$$= \begin{bmatrix} \cos(pL) & -\sin(pL) & 0 & 0 \\ \sin(pL) & \cos(pL) & 0 & 0 \\ 0 & 0 & \cos(pL) & -\sin(pL) \\ 0 & 0 & \sin(pL) & \cos(pL) \end{bmatrix} \tag{16}$$

$$\left[\underline{\underline{C}}(L)\right] = \begin{bmatrix} e^{ig_1 L} & 0 & 0 & 0 \\ 0 & e^{ig_2 L} & 0 & 0 \\ 0 & 0 & e^{-ig_1 L} & 0 \\ 0 & 0 & 0 & e^{-ig_2 L} \end{bmatrix}, \tag{17}$$

$$\left[\left(\underline{\underline{T}}\right)\right] = \begin{bmatrix} e_{11} & e_{21} & e_{11} & e_{21} \\ e_{12} & e_{22} & -e_{12} & e_{22} \\ h_{11} & h_{21} & h_{11} & h_{21} \\ h_{12} & h_{22} & -h_{12} & -h_{22} \end{bmatrix}, \tag{18}$$

When the reflectance and transmittance amplitudes are determined one can obtain the reflectance and transmittance coefficients using:

$$r_{ij} = \frac{r_i}{a_j}, \qquad i,j = L,R$$
$$t_{ij} = \frac{t_i}{a_j}, \qquad i,j = L,R \tag{19}$$

The transmittance coefficients for plane waves of s and p polarization can easily be obtained from Eq. [9]:

$$\begin{cases} t_{SS} = \frac{(t_{LL} + t_{RR}) - (t_{LR} + t_{RL})}{2} \\ t_{SP} = -i\frac{(t_{LL} + t_{RR}) - (t_{LR} - t_{RL})}{2} \\ t_{PS} = i\frac{(t_{LL} - t_{RR}) - (t_{LR} - t_{RL})}{2} \\ t_{PP} = \frac{(t_{LL} + t_{RR}) - (t_{LR} + t_{RL})}{2} \end{cases}, \tag{20}$$

The incidence and transmittance ellipticities are denoted by:

$$\Psi_{inc} = \frac{-2im\left[a_s a_p^*\right]}{\left(|a_s|^2 + |a_p|^2\right)}, \tag{21}$$

and,

$$\Psi_{inc} = \frac{-2im\left[t_s t_p^*\right]}{\left(|t_s|^2 + |t_p|^2\right)}, \tag{22}$$

where Im[ ] defines the imaginary part.

Optical activity is the angle that occurs because of the rotation of the long axis of the transmittance vibrational ellipsoid with respect to the long axis of the incident vibrational ellipsoid. In order to calculate the optical activity (optical rotation) the following auxiliary vectors are introduced [16]:

$$\underline{F}_{inc} = \left[1 + \left(1 - \Psi_{inc}^2\right)^{\frac{1}{2}}\right] Re\left[a_s \underline{u}_y - a_p \underline{u}_x\right] - \Psi_{inc} Im\left[a_s \underline{u}_x + a_p \underline{u}_y\right], \tag{23}$$

$$\underline{F}_{tr} = \left[1 + \left(1 - \Psi_{tr}^2\right)^{\frac{1}{2}}\right] Re\left[t_s \underline{u}_y - t_p \underline{u}_x\right] - \Psi_{tr} Im\left[t_s \underline{u}_x + t_p \underline{u}_y\right], \tag{24}$$

where Re[ ] defines the real part.

Then the tilt angles τ_{tr} and τ_{inc} can be calculated from:

$$\cos\tau_l = \frac{\underline{F}_l \cdot \underline{u}_y}{|\underline{F}_l|},$$
$$\sin\tau_l = \frac{-\underline{F}_l \cdot \underline{u}_x}{|\underline{F}_l|}, \qquad (l = inc, tr) \tag{25}$$

and the optical activity as [16,17]:

$$\phi_{tr} = \begin{cases} \tau_{tr} - \tau_{inc} + \pi, & if \quad -\pi \le \tau_{tr} - \tau_{inc} \le -\pi/2 \\ \tau_{tr} - \tau_{inc}, & if \quad |\tau_{tr} - \tau_{inc}| \le \pi/2 \\ \tau_{tr} - \tau_{inc} - \pi, & if \quad \pi/2 \le \tau_{tr} - \tau_{inc} \le \pi. \end{cases} \tag{26}$$

Calculation of ϕ_{rr} may result in $|\phi_{rr}| > \pi/2$, in that case a value of - π should be added to the ϕ_{rr} value. On the other hand if the calculated value is $|\phi_{rr}| \prec -\pi/2$ then π should be added. This procedure confines the value of ϕ_{rr} in the range of $\left[-\pi/2, \pi/2\right]$.

3. Numerical results and discussions

Consider a right handed chiral sculptured copper thin film that has occupied the free space (vacuum) with a thickness of d and that this copper film is formed in its bulk state. In order to obtain the relative permittivity scalars $\varepsilon_{a,b,c}$ in sculptured thin films we used the Bruggemen homogenization formalism. In this for-
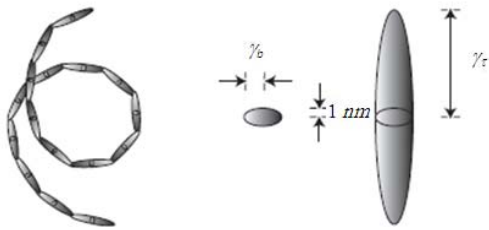
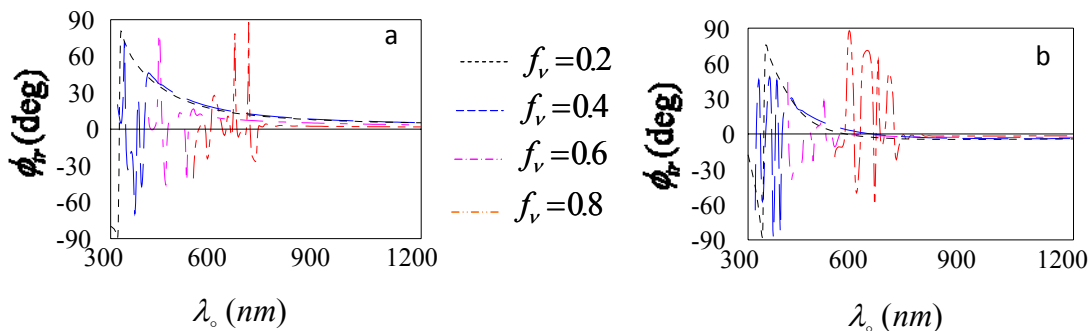**Fig. 2. A STF column which is considered as a string of identical long electrical ellipsoids with shape factors γ_b and γ_τ.**

100 nm [18,19]. Homogenization was only performed for the 590.38 nm wavelength with a relative permittivity -7.67+2.63i [20]. It was assumed that the vacuum topology is the same as that of metal (i.e., $\gamma_b^s = \gamma_b^v, \gamma_\tau^s = \gamma_\tau^v$). Hence the relative permittivity scalars remain fixed by changing the wavelength. After calculation of relative permittivity scalars from Bruggeman homogenization formalism one can obtain the reflectance and transmittance amplitudes using matrix equation (1).

In Fig. 3 the optical activity of a right handed chiral sculptured copper thin film in axial propagation for both s and p polarizations is depicted. In Figs. 3-a and 3-b, $\gamma_\tau^s = \gamma_\tau^v = 10$ nm, $\gamma_b^s = \gamma_b^v = 1$ nm, $\chi = 30°$, Ω

Fig. 3. Optical activity of a right handed chiral sculptured copper thin film in axial propagation for both s and p polarizations with different volume fractions.
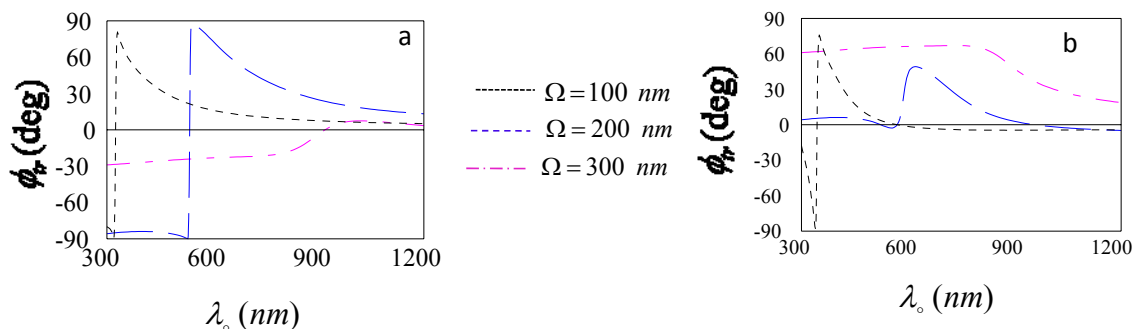
Fig. 4. Optical activity of a right handed chiral sculptured copper thin film in axial propagation for both s and p polarizations with different structural periods.

malism the film is considered to be formed as a composite of two phases, namely vacuum phase and the matter phase. These quantities depend on the column shape, volumetric fraction of vacuum phase, free space wavelength and relative permittivity of the matter (inclusion). Each column in the sculptured thin film is considered to consist of a string of small and identical ellipsoids and electrically small (i.e., small in a sense that their electrical interaction can be ignored) (Fig. 2) [10]. In Fig. 2 $\gamma_\tau^{s,v}$ is one half of the long axis of the inclusion and void ellipsoids, and $\gamma_b^{s,v}$ is one half of the small axis of the inclusion and void ellipsoids. It should be mentioned that these parameters which define the shape factor range between 1 and

= 100 nm and d = 1000 nm were fixed. In these figures it can be observed that the optical activity for both s and p polarizations shifts to longer wavelengths with increasing the volume fraction of the copper inclusions. Therefore, the location of occurrence of circular Bragg phenomenon (position of maximum of optical activity) shifts towards longer wavelengths.

In these figures some instabilities occur in the numerical calculations for higher values of volume fraction of metallic inclusions (greater than 0.2) and at shorter wavelengths, which are either higher or lower than the limit of accuracy which can be handled by the computer and they should be avoided.
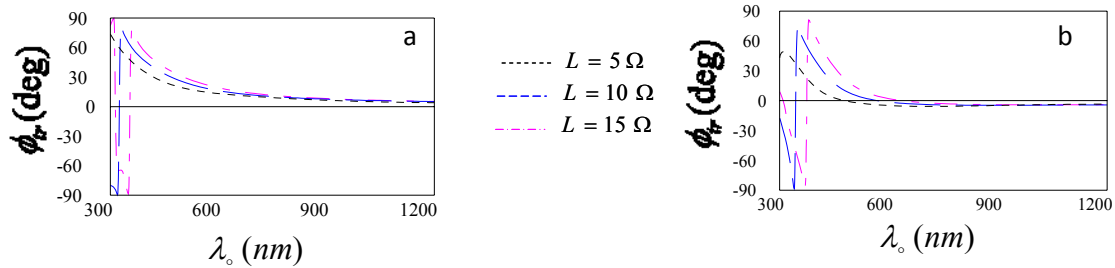
Fig. 5. Optical activity of a right handed chiral sculptured copper thin film in axial propagation for both s and p polarizations with different thickness.
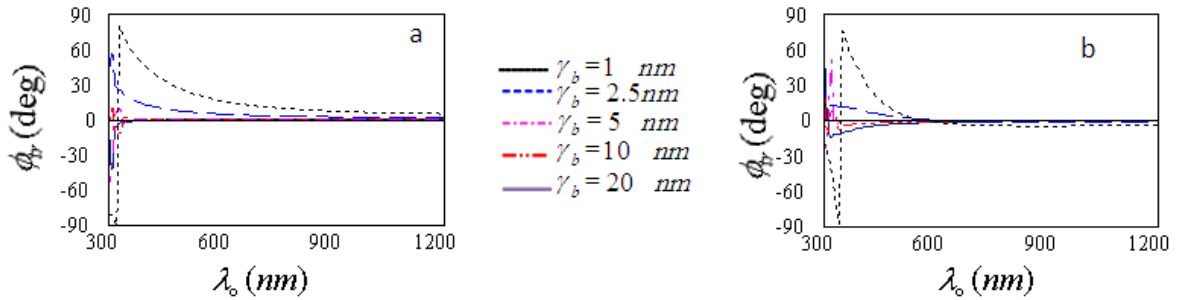

Fig. 6. Optical activity of a right handed chiral sculptured copper thin film in axial propagation for both s and p polarizations with different transverse aspect ratio of the columns.

Optical activity was calculated for $\gamma_\tau^s = \gamma_\tau^v = 10$ nm, $\gamma_b^s = \gamma_b^v = 1$ nm, $\chi = 30°$, $f = 0.2$ and $d = 1000$ nm in Figs. 4-a and 4-b. It can be seen that the maximum of the optical activity shifts to longer wavelengths with increasing the half structural period. This is because the light should at least travel (pass through) one structural period until the circular Bragg phenomenon occurs.

Figs. 5-a and 5-b show the results of optical activity calculations for, $\gamma_\tau^s = \gamma_\tau^v = 10$ nm, $\gamma_b^s = \gamma_b^v = 1$ nm, $\chi = 30°$, $\Omega = 100$ nm and $f = 0.2$. In these figures it can also be observed that the maximum of the optical activity for both s and p polarizations shifts to longer wavelengths with increasing the film thickness.

This is due to the fact that the number of Bragg reflecting planes increase with increasing the film thickness.

In Figs. 6-a and 6-b, $\gamma_\tau^s = \gamma_\tau^v = 10$ nm, $\Omega = 100$ nm, χ

$= 30°$, $f = 0.2$ and $d = 1000$ nm were fixed. It is obvious that the maximum of the optical activity for both s and p polarizations shifts to shorter wavelengths with increasing the transverse aspect ratio of the columns. This results because in axial excitation of CSTFs in which the propagation direction of light is parallel to the inhomogeneity axis of sculptured thin film (parallel to z-axis) the needle like form of nano-wires disappears.

Figs. 7-a and 7-b are the results of optical activity calculations for $\gamma_\tau^s = \gamma_\tau^v = 10$ nm, $\gamma_b^s = \gamma_b^v = 1$ nm , $\Omega = 100$ nm, $f = 0.2$ and $d = 1000$ nm. It can be seen that the intensity of the maximum of the optical activity for both s and p polarizations decreases with increasing the rise angle and the circular Bragg phenomenon disappears. Therefore, if one requires to use the circular Bragg phenomenon in a particular application, the lower rise angles are more appropriate.
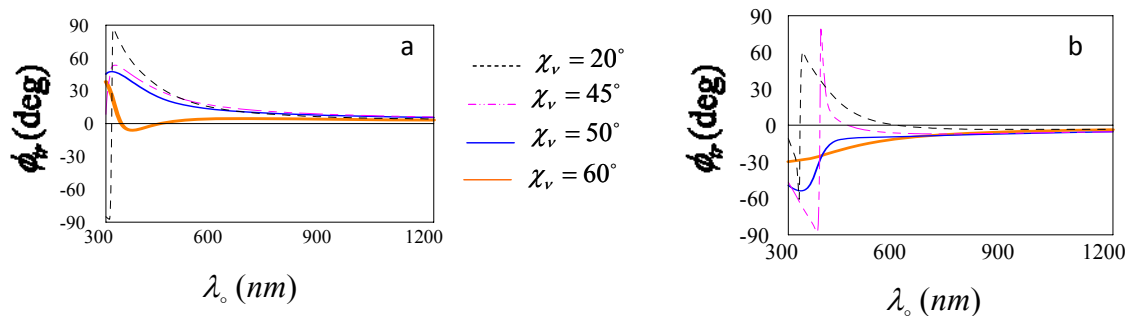

Fig. 7. Optical activity of a right handed chiral sculptured copper thin film in axial propagation for both s and p polarizations with different angle of rise of the columns.
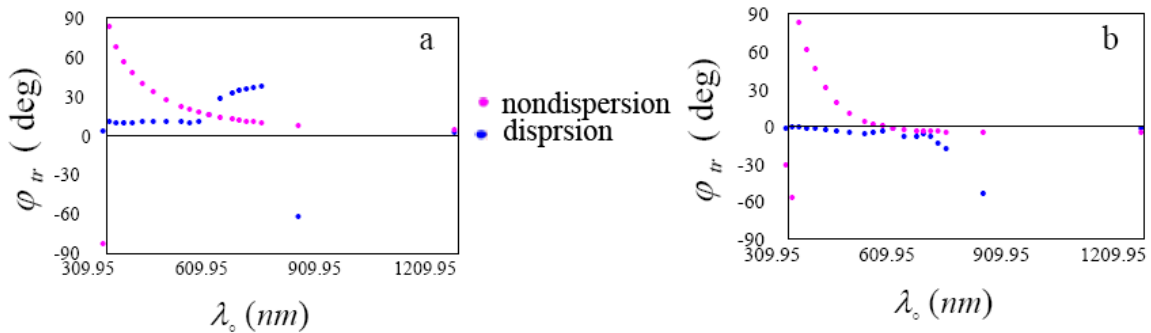
Fig. 8. Optical activity of a right handed chiral sculptured copper thin film in axial propagation for both s and p polarizations compared for dispersion and nondispersion of the dielectric function.

Results of optical activity for $\gamma_\tau^s = \gamma_\tau^v = 10$ nm, $\gamma_b^s = \gamma_b^v = 1$ nm, $\Omega = 100$ nm, $\chi = 30°$, f = 0.2 and d = 1000 nm are depicted in Figs. 8-a and 8-b. In these figures it can be seen that optical activity spectra for both s and p polarizations is considerably affected by dispersion of dielectric function and its effect is more significant at shorter wavelengths.

In summary, the Bruggman homogenization formalism and the eigenvalue method were used in conjunction with experimental results for dielectric function of copper in bulk state and calculated the optical activity of chiral sculptured copper thin films when different structural parameters were varied.

4. Conclusions

Optical activity spectra of chiral sculptured copper thin films are studied, using Bruggman homogenization formalism and eigenvalue method. Results show that the maximum of the optical activity shifts toward longer wavelength with increasing structural period, volume fraction of metal inclusion and film thickness, while it shifts toward shorter wavelengths with increasing transverse aspect ratio of columns. Also optical activity decays at larger rise angles. Results also show that at short wavelengths one cannot ignore the dispersion of the dielectric function.

Acknowledgements

References

[1]   K. Robbie, G. Beydaghyan, T. Brown, C. Dean, J. Adams, C. Buz, Rev. Sci. Instrum., **75,** 1089 (2004).

[2]   O. N. Singh, A. Lakhtakia, Electromagnetic Fields in Unconventional Materials and Structures (Wiley, New York, 2000) p. 151.

[3]   Q. Wu, I. J. Hodgkinson, A. Lakhtakia, Opt. Eng., **39,** 1863 (2000).

[4]   A. Lakhtakia, Opt. Eng. **38**, 1596 (1999).

[5]   I. J. Hodgkinson, A. Lakhtakia, Q. h. Wu, Opt. Eng., **39,** 2831 (2000).

[6]   A. Lakhtakia, M. W. McCall, J. A. Sherwin, Q. H.Wu, I. J. Hodgkinson, Opt. Commun. **194,** 33 (2001).

[7]   I. J. Hodgkinson, Q. H. Wu, A. Lakhtakia, M. W. McCall, Opt. Commun **177,** 79 (2000).

[8]   I. J. Hodgkinson, Q. H. Wu, K. E. Thorn, A. Lakhtakia, M. W.McCall, Opt. Commun. **184,** 57 (2000).

[9]   K. Robbie, M. J. Brett and A. Lakhtakia, Nature **384,** 616 (1996).

[10]   A. Lakhtakia and R. Messier, Sculptured thin films, Nanoengineered Morphology and Optics (SPIE, USA, 2005) Chap. 9.

[11]   F. Babaei and H. Savaloni, Opt. Commun., **278,** 321 (2007).

[12]   F. Babaei, H. Savaloni, Opt. Commun., **278,** 221 (2007).

[13]   J. A. Sherwin, A. Lakhtakia, Math Comput. Model. **35,** 1355 (2002).

[14]   J. A. Sherwin, A. Lakhtakia, I. J. Hodgkinson, Opt. Commun. **209,** 369 (2002).

[15]   V. C. Venugopal, A. Lakhtakia, Proc. Royal Soc. Lond. **A 454,** 1535 (1998).

[16]   J. A. Sherwin, A. Lakhtakia, Opt. Commun., **214,** 231 (2002).

[17]   J. A. Sherwin, A. Lakhtakia, Opt. Commun., **222,** 305 (2003).

[18]   A. Lakhtakia, Microw. Opt. Technol. Lett. **24** (2000) 239.

[19]   F. Wang, PhD Thesis, University of Pennsylvania, (2005).

[20]   E. D. Palik, Handbook of Optical Constants of Solids, Academic press, Newyork, (1985).